Theories of Multiple Equilibria–A Critical Reexamination. Part I: Barotropic Models

K. K. TUNG AND A. J. ROSENTHAL*

Mathematics Department, Massachusetts Institute of Technology, Cambridge, MA 02139

(Manuscript received 17 September 1984, in final form 26 July 1985)

ABSTRACT

Previous results claiming the existence of multiple equilibria based on simple barotropic or two-layer models of the atmosphere are reexamined. While not ruling out the existence of multiple equilibria we find that the application of these results to the atmosphere, especially with regard to high/low zonal index and zonal/blocked situations, is probably problematic. Results based on truncated low-order models are found to change drastically when full nonlinearity is retained. Although multiple equilibria may still exist in some nonlinear models in some restricted parameter regimes, it is argued that the parameter values adopted in previous studies are probably not physically based.

Mathematically interesting properties of the nonlinear system, such as resonance bending, hysteresis, bifurcation and multiplicity of solutions are also discussed.

1. Introduction

Based on a highly truncated spectral model of a barotropic atmosphere, Charney and DeVore (1979, hereafter referred to as CD) suggested that there may exist a multiplicity of distinct equilibrium states for large-scale flow patterns in the atmosphere for a given external driving. In particular, a low zonal index, high wave amplitude state may coexist with a high zonal index, low wave amplitude state, suggestive of blocked and unblocked flow patterns sometimes observed in the atmosphere. Similar results were also obtained by Wiin-Nielsen (1979) using a low-order model on the sphere.

The existence of multiple equilibria appears to have been substantiated by, for example, Hart (1979), Trevisan and Buzzi (1980), Charney *et al.* (1981), Pedlosky (1981a,b), Källén (1981, 1982), Legras and Ghil (1984, 1985), and Yoden (1985) for the barotropic case, and Charney and Straus (1980), Roads (1980a,b; 1982), Pedlosky (1981b), Yoden (1983a), and Källén (1983) using two-layer models.[1] There is probably little doubt that multiple equilibria exist in *some parameter regimes* (namely, for high enough mountains, low enough viscosity and strong enough "thermal forcing") at least in barotropic models, and perhaps also in baroclinic models if the concept of equilibrium state is modified slightly. The issue we wish to address here is: Given realistic magnitudes of topographic elevation, physically based zonal driving and Ekman damping, do multiple equilibria still exist? We wish to address this issue with a fully nonlinear model and compare our result with the ones previously obtained from low-order models.

There has been an attempt by Charney *et al.* (1981, hereafter referred to as CSM) to show that at least three equilibria exist in a severely truncated barotropic model even when a realistic distribution of topography is used. We will first show, using the same topographic forcing, that the state of multiple equilibria disappears when nonlinearity is incorporated by including more wave modes until convergence is achieved.

A comprehensive study of the nonlinear barotropic vorticity equation with one-mode topography was undertaken by Legras and Ghil (1984, 1985), using a less severely truncated model than CD (with 25 modes retained in the solution). Their result suggests that the parameter domain in which multiple equilibria are present is greatly reduced when nonlinearity is properly taken into account. This property of the barotropic solution was previously pointed out by Davey (1980, 1981), whose "improved quasi-linear" solution, which takes into account the interaction between waves and mean *shear*, has a narrower domain for which multiple equilibria exist than his "quasi-linear" solution, which incorporates only the interaction between waves and the overall net zonal flow. (CSM's truncated solution can be called "quasi-linear" according to this terminology.) The recent result of Rambaldi and Mo (1984) reconfirmed Davey's finding concerning the importance of wave–mean shear interaction.

According to Legras and Ghil (1985), the nonlinear (i.e. less severely truncated) counterpart of CD's result of 3 equilibria now occurs when their nondimensional parameter ρ exceeds ~ 0.5 (at a damping time of 5.25

[1] However, for the latter case the meaning of "equilibrium" needs to be modified (see Tung and Rosenthal, 1985). We will return to this point in Part II.

* Present affiliation: Mathematics Department, Salem State College, Salem, MA 01970.

days). The parameter ρ used by Legras and Ghil measures the strength of the zonal driving Ψ^* (in the notation of CD), and $\rho = 0.5$ corresponds to a barotropic zonal jet with a 150 m s^{-1} speed.

The more recent results mentioned above suggest that *nonlinear* solutions of the barotropic vorticity equation can possess multiple equilibria, but these now occur in a different, perhaps less realistic, part of the parameter regime. The determination of what constitutes a "realistic" regime in a barotropic model of the atmosphere is, however, rather problematic. By starting with a general three-dimensional baroclinic atmosphere, we will attempt to give a physical interpretation of the so-called "thermal forcing" terms used in barotropic models. This allows us to estimate their order of magnitude from observational data.

It is more difficult to decide what magnitude of viscous damping time-scale should be used in barotropic models. A commonly used value for damping time based on Ekman boundary layer parameterization is about 6 days (Charney and Eliassen, 1949). This value is also consistent with the 5 days value obtained by interpreting the damping time as a characteristic residence time of the vertically averaged kinetic energy in the atmosphere (Kanamitsu, 1981). Longer damping times have also been adopted by some authors from time to time. For example, CSM used 14.3 days, and Rambaldi and Mo (1984) 15 days. Realizing the controversial nature of choosing a "correct" value of damping to use in barotropic models, we will instead perform calculations using a *range* of damping time scales, from 5 days to 30 days, and discuss the dependence of the solution on this and other parameters. Our results do not appear to support the conclusion of multiple distinct equilibria of the large-scale flow even for small dampings.

2. A reexamination of the model of CSM

The paper by CSM is important because it appears to be the only attempt to show that the theoretical result of multiple equilibria is relevant to an atmosphere with realistic distribution of topography and with a damping time based on a parameterization of the Ekman boundary layer having a value independently determined by Charney and Eliassen (1949, hereafter referred to as CE).

For the barotropic model in a β-plane channel the governing potential vorticity equation is, in dimensionless form:

$$\frac{\partial}{\partial t}\nabla^2\Psi + J[\Psi, \nabla^2\Psi + \beta y] = -J(\Psi, h) - k\nabla^2(\Psi - \Psi^*), \quad (2.1)$$

where, following CSM we have nondimensionalized x and y by L (where πL is the channel width), t by f_0^{-1}, Ψ by f_0/L and h by H_0. [Ψ is the quasi-geostrophic stream function; $k\nabla^2\Psi^*$ the externally imposed vorticity source; h the topographic elevation and H_0 the scale height.] The dimensionless Ekman damping parameter k is defined by

$$k \equiv \frac{1}{H_0}\left(\frac{\nu_E}{2f_0}\right)^{1/2}, \quad (2.2)$$

with ν_E being the bulk eddy viscosity. CE found that

$$\nu_E = K\sin^2 2\delta \sim 5 \text{ m}^2 \text{ s}^{-1}, \quad (2.3)$$

(where K is the "eddy-diffusivity" and δ is the angle between the isobars and the surface wind) corresponding to an Ekman damping time scale

$$\tau_E \equiv \frac{2H_0}{f_0(2\nu_E/f_0)^{1/2}} \quad (2.4)$$

of about 6 days, and a dimensionless damping parameter of

$$k \approx 0.02. \quad (2.5)$$

To obtain the equation for the mean flow, we take the zonal average of the second y-integral of Eq. (2.1) to get

$$\frac{\partial}{\partial t}U = k(U^* - U) + \mathrm{T}, \quad (2.6)$$

where

$$U \equiv \frac{1}{(y_2 - y_1)}\int_{y_1}^{y_2} \bar{u}dy = \frac{1}{y_2 - y_1}[\bar{\Psi}|_{y_1} - \bar{\Psi}|_{y_2}] \quad (2.7)$$

is the zonal index for the flow between y_1 and y_2, and measures the net geostrophic flow in the east–west direction inside the channel,

$$\mathrm{T} \equiv \frac{1}{y_2 - y_1}\int_{y_1}^{y_2} \overline{\Psi_x h}dy \quad (2.8)$$

is called the mountain torque, and

$$U^* \equiv \frac{1}{y_2 - y_1}[\Psi^*|_{y_1} - \Psi^*|_{y_2}] \quad (2.9)$$

represents the zonal momentum driving for the flow inside the channel.

In the absence of mountains (i.e. $h \equiv 0$), (2.6) implies that the flow would relax into

$$U = U^*.$$

Thus U^* can also be interpreted as the net zonal flow for the Hadley circulation in the channel.

CSM assumed that Ψ^* is a linear function of y, i.e.

$$\Psi^* = -U^* y, \quad (2.10)$$

so that the so-called "thermal" driving Ψ^* shows up not as a vorticity source in (2.1) but as a momentum driving for the mean zonal flow in (2.6). The same assumption is used by Rambaldi and Mo (1984), but

not by Legras and Ghil (1984, 1985). We will come back to this point later.

Equilibrium solutions are found by solving (2.1) and (2.6) subject to the boundary condition that the meridional component of the geostrophic velocity vanishes at the channel boundaries, i.e.

$$\frac{\partial}{\partial x}\Psi = 0 \quad \text{at} \quad y_1 \quad \text{and} \quad y_2. \tag{2.11}$$

Equation (2.11) implies that Ψ is a constant at y_1 and another constant at y_2. The difference between the two constants measures the total mass flow inside the channel, according to (2.7). Without loss of generality, we can set Ψ at y_1 to be zero, and replace (2.11) by

$$\Psi = \begin{cases} 0 & \text{at} \quad y_1 = 0 \\ -U\pi & \text{at} \quad y_2 = \pi. \end{cases} \tag{2.12}$$

Since the stationary wave solution to (2.1), subject to the lateral boundary condition (2.12) depends on U, it then follows that the mountain torque is also a function of U, i.e.,

$$\mathrm{T} = \mathrm{T}(U). \tag{2.13}$$

Once $\mathrm{T}(U)$ is found from the solution of (2.1) (without the time derivative) for different values of U, the equilibrium solution to the system is obtained by solving for the U that satisfies:

$$k(U^* - U) = -\mathrm{T}(U). \tag{2.14}$$

Since according to (2.12), $\Psi + U\cdot y$ vanishes at $y = 0$ and π, that quantity can be represented in general by a sine series as (with $N \to \infty$, $M \to \infty$)

$$\Psi + U\cdot y = \sum_{n=1}^{N} \phi_n(x, t) \sin ny, \quad 0 < y < \pi \tag{2.15}$$

with

$$\phi_n(x, t) = \mathrm{Re} \sum_{m=0}^{M} \phi_{mn} e^{im\alpha x}, \quad 0 \leqslant \alpha x \leqslant 2\pi$$

if the solution is assumed to be periodic along a zonal circle ($\alpha \equiv L/(a\cos\theta_0$, where a is the earth's radius and we take $\theta_0 = 45.$). The topographic distribution of the earth's surface is expanded in a similar manner

$$h = \sum_{n=1}^{N} h_n(x) \sin ny, \quad 0 < y < \pi \tag{2.16}$$

with

$$h_n(x) = \mathrm{Re} \sum_{m=0}^{M} h_{mn} e^{im\alpha x}, \quad 0 \leqslant \alpha x \leqslant 2\pi.$$

Substituting (2.15) and (2.16) into the barotropic vorticity equation (2.1) and setting the time derivative in that equation to zero yields the following nonlinear equation in dimensional form for the wave amplitude ϕ_{mn}

$$\sum_{\bar{m}=-M}^{M} \sum_{\bar{n}=-N}^{N} (m\bar{n} - \bar{m}n)\phi_{\bar{m}\bar{n}} q_{m-\bar{m},n-\bar{n}} (\delta_{\bar{m},0} + 1)$$
$$= 4ULmq_{mn} + 4L\beta m\phi_{mn}$$
$$+ 4i \frac{1}{\tau_E}\left(\alpha m^2 + \frac{n^2}{\alpha}\right)(\delta_{m,0} + 1)\phi_{mn} \tag{2.17}$$

where

$$\mathrm{Im}h_{on} = 0, \quad h_{-m,n} = \text{c.c. of } h_{m,n},\ h_{m,-n} = -h_{m,n},$$

and similarly for ϕ_{mn};

$$q_{mn} = (\delta_{m,0} + 1)\left[\frac{H_0}{f_0} h_{mn} - \frac{(\alpha m^2 + n^2/\alpha)}{aL\cos\theta_0}\right]$$

and $\delta_{m,\bar{m}} = 1$ if $m = \bar{m}$, 0 otherwise. This nonlinear algebraic equation is solved numerically using Newton's method with arc-length continuation (Keller, 1977; Rheinboldt and Burkardt, 1983a,b). The numbers of modes used are $M = 15$ (in the zonal direction) and $N = 4$ (in the meridional direction), although higher resolution (with $M = 30$; $N = 8$) has in some cases been used to check for convergence.

In CSM, N is truncated to 1, resulting in a linear equation for ϕ_1 (the same as that used by CE):

$$\frac{\partial}{\partial t}(\phi_{1xx} - \phi_1) + U(\phi_{1xxx} - \phi_{1x}) + \beta\phi_{1x}$$
$$= -k(\phi_{1xx} - \phi_1) - Uh_{1x}. \tag{2.18}$$

The mountain torque is found to be given by

$$\mathrm{T}(U) = \frac{1}{\pi}\int_0^{\pi} \overline{\phi_{1x}h_1} \sin^2 y dy$$
$$= \frac{1}{4}\overline{(h_1\phi_{1x} - \phi_1 h_{1x})}. \tag{2.19}$$

{Due to minor algebraic error, CSM has a factor of $\frac{1}{3}$ instead of $\frac{1}{4}$ in front of $(h_1\phi_{1x} - \phi_1 h_{1x})$ in (2.19) [cf. their Eq. (3)]. The error arises because their counterpart to our (2.6) was obtained by multiplying (2.1) by cos$y$ and then integrating across the channel width. This procedure should have yielded "zero = zero".}

In addition to truncating N to be 1, CSM made a further equivalent barotropic assumption, which involves multiplying the topographic ($h-$) term in wave equation (2.18) and the damping ($k-$) term in the mean flow equation (2.14) by the factor $\kappa = 0.4$. Nevertheless, the two κ cancel each other in the final equation for the determination of the equilibrium U [their Eq. (7)], which does not contain any κ factors. Therefore the use of (2.18) and (2.14) without the κ should produce the same (truncated) equilibrium U-solution as in CSM for the same value of k. (There is, however, a slight difference in the nonlinear solution.)

The result by CSM for $-\mathrm{T}(U)$ versus U is reproduced in Fig. 1 using the topographic components listed in

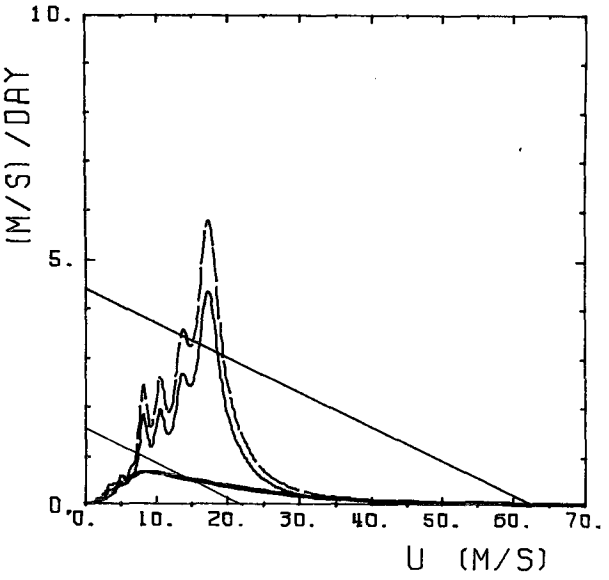

FIG. 1. Mountain torque (−T) in m s^{-1}/day, as a function of U (m s^{-1}), calculated using the topographic modes tabulated by Charney *et al.* (1981) for a dimensionless damping parameter of $k = 0.008$, corresponding to an Ekman damping time-scale of $\tau_E = 14.3$ days. Top dashed curve: Linear solution of CSM with the (incorrect) factor of $\frac{1}{3}$. Second solid curve: Linear solution with the (correct) factor of $\frac{1}{4}$. Bottom solid curve: Nonlinear solution. Straight line sloping downward to the right: $\tau_E^{-1}(U^* - U)$, shown with $U^* = 63$ m s^{-1} and $U^* = 22$ m s^{-1}.

CSM's Fig. 1, and for $k = 0.008$, corresponding to a 14.3-day damping time-scale. They used this smaller value of damping although it was claimed in CSM that the same bulk eddy viscosity as in (2.3) was used. The top dashed curve is calculated in the same way as in CSM with the (incorrect) $\frac{1}{3}$ factor in the expression for the mountain torque (2.19). The middle solid curve is the correct quasi-linear solution, calculated with the $\frac{1}{4}$ factor in (2.19). The lowest solid curve represents the mountain torque calculated without severe truncation in the solution but using the same topography. [Note that the topography modes listed in CSM have only one y-mode, but the nonlinear solution calculated here is allowed to have many y-modes.] The truncated solution using CSM topography and the incorrect $\frac{1}{3}$ factor shows 5 equilibria, 3 of which are stable as discussed by CSM. The high zonal index stable equilibrium, with $U \approx 63$ m s^{-1}, is not realizable in the real atmosphere, where the net zonal wind seldom exceeds 30 m s^{-1} (at the "equivalent barotropic level"). The other two stable equilibria, corresponding to a subresonant wavenumber 2 solution and a subresonant wavenumber 3 solution, occur at more reasonable U. When the algebraic error involving the $\frac{1}{3}$ factor is corrected, only one of the "attainable" equilibria, the subresonant wavenumber 2 solution, remains when $U^* = 63$ m s^{-1}. Nevertheless, if U^* is changed to 47 m s^{-1}, multiple equilibrium states similar to those discussed by CSM reappear.

The solution calculated without severe truncation has a peak mountain torque which is more than 6 times smaller than the truncated solution of CSM. The dramatic change from linear to nonlinear solutions is due mainly to the fact that a significant fraction of the wave energy is transferred to the wavenumber zero component in the nonlinear case, producing *shears* in the mean zonal wind (Davey, 1980; 1981) but contributing to no mountain torque. Also, nonlinear resonant solutions in the presence of damping that is as small as used for this case tend to have wave amplitudes that are a few times smaller than those of the linear solutions. (see Fig. 7 to be discussed later.)

The important conclusion from Fig. 1 is that when the CSM solution is repeated without severe truncation, *there is only one equilibrium for any value of the external parameter* U^* in the nonlinear solution. Thus it is seen that the multiple equilibria seen in the truncated solution are merely artifacts of the severe truncation used.

In Fig. 2, we present results calculated using the Scripps topography as tabulated by Gates and Nelson (1975). The 1° × 1° grid-point data are Fourier analyzed according to (2.16) with $M = 15$ and $N = 8$ for a channel extending from 30°N to 63° (to facilitate comparison of our results with those of CSM). Since the Fourier components derived from the Scripps topography tend to have slightly larger magnitudes than the CSM topography, the calculated solutions also tend to have slightly larger amplitudes. A more significant difference is that there are many y-modes in the topographic forcing when the Scripps topography is used, and there is only 1 y-mode in the topography taken from the table in CSM. The presence of more y-mode forcing tends to produce more small-scale fine structures in the solution, as will be discussed in a moment.

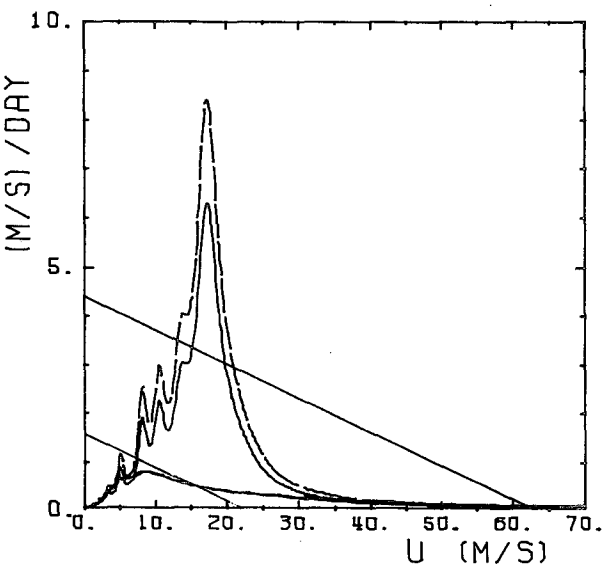

FIG. 2. As in Fig. 1 except that the Scripps topography is used.

Visual inspection of Fig. 2 suggests that again there are *no distinct multiple equilibrium states in the nonlinear solution.* The word "distinct" should be emphasized here, for in the presence of small-scale topographic modes, the calculated mountain torque curve has complicated fine structures at low values of U. This is not apparent in the scale used in Fig. 2 but becomes clearer when the portion of Fig. 2 between $U = 4$ and $U = 8$ m s^{-1} is enlarged many times. This is shown in Fig. 3 for the nonlinear solution only. The complicated fine structure makes it possible in principle for ten or more equilibria to exist for some fixed values of U^*. However, these equilibria are not the kind of distinct large-scale (e.g. high/low index, blocked/unblocked) states envisaged by CD, because they differ from each other only in some small-scale structures. These fine structures are caused by the small-scale modes present in the topography, and disappear when we eliminate the higher meridional modes in the Fourier decomposition of topography (but no such truncation is adopted when solving for the ϕ_{mn} in the nonlinear solution). This is shown in Fig. 4 for the nonlinear solution calculated with a (15, 1) form of Scripps topography.

The fine-structure behavior mentioned above also disappears when the damping time-scale used in the model is decreased. The calculation is repeated using the same (untruncated) Scripps topography but with a damping time of 5.7 days ($k = 0.02$), corresponding to (2.4) and (2.5) suggested by CE. While the linear solution possess 3 (and not more than 3) equilibria for some particular U^* ($U^* \sim 33$ m s^{-1}), *there is only one equilibrium in the nonlinear solution,* as seen in Fig. 5.

For this larger value of damping (i.e., 5.7 days instead of 14.3 days damping time), the difference between linear and nonlinear solutions is less dramatic. The multiple peaks and valleys in the linear mountain torque curve that we have seen at $k = 0.008$ mostly disappear now at the larger damping parameter of $k = 0.02$. (This does not imply, however, that there is no resonance. Different wavenumber solutions still respond preferentially for certain resonant values of U.)

Figure 6 shows the equilibrium geopotential height of the nonlinear wave solution to (2.1) as a solid curve

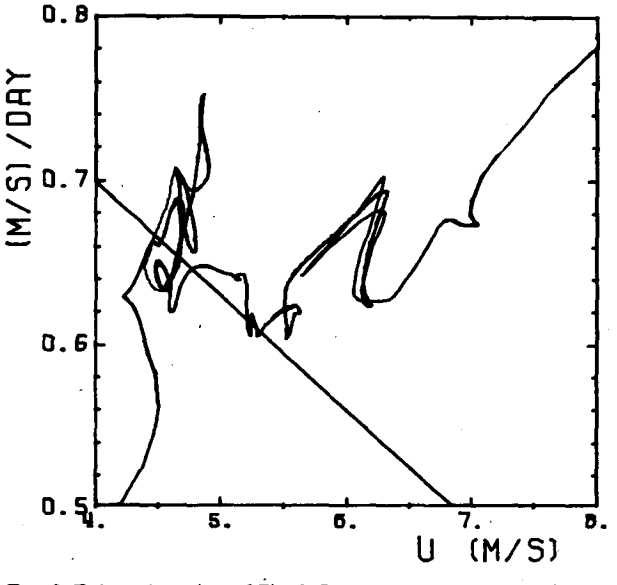

FIG. 3. Enlarged portion of Fig. 2. The curve shows the nonlinear solution and the straight line shows $\tau_E^{-1}(U^* - U)$.

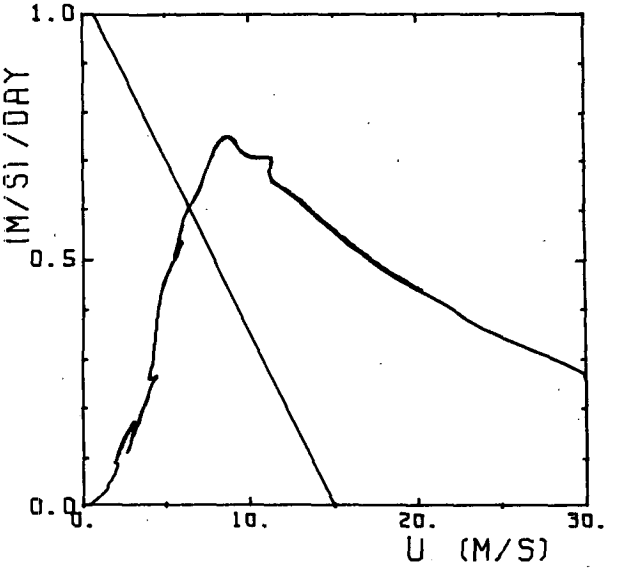

FIG. 4. As in Fig. 2 except that only the first y-mode in the Fourier decomposition of the Scripps topography is used to obtain the nonlinear solution shown.

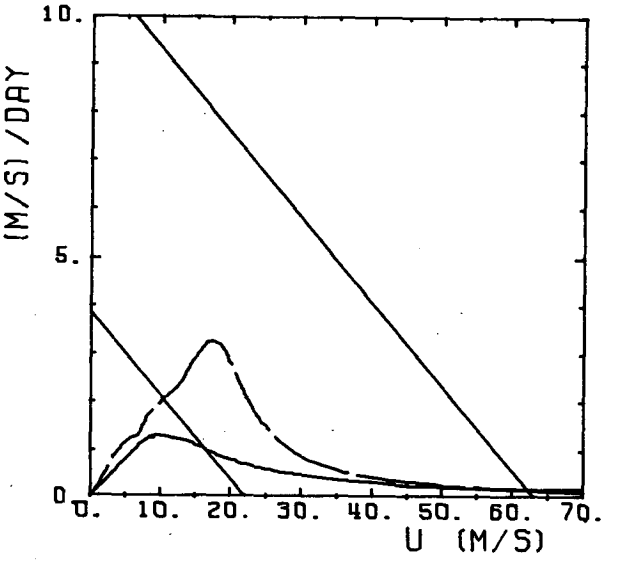

FIG. 5. As in Fig. 2 except for a larger damping parameter of $k = 0.02$, corresponding to an Ekman damping time-scale of $\tau_E = 5.7$ days. Here the dashed curve represents the (correct) linear solution for (−T), while the solid curve is the (converged) nonlinear solution.

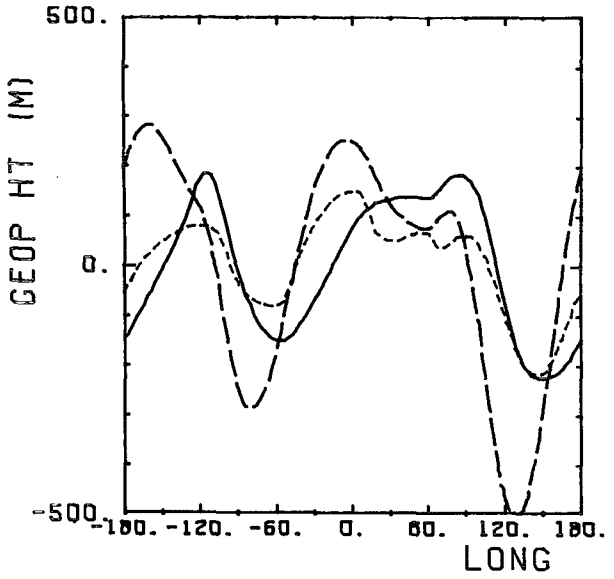

FIG. 6. Wave geopotential height (in meters) at 45°N vs longitude for $\tau_E = 5.7$ days and $U = 15$ m s^{-1}, which is the equilibrium solution for $U^* = 22$ m s^{-1}. The solid curve shows the nonlinear solution, the curve with long dashes shows the linear solution and the curve with short dashes shows the observed climatological 500 mb eddy geopotential height at 45°N in January, from Oort (1983).

(for 5.7 days damping time). The observed climatology at 500 mb and 45°N in January from Oort (1983) is shown as a curve with short dashes. The curve with long dashes is the linear solution. The discrepancy between the linear and nonlinear solutions is not as great as what we have found for the 14.3 day damping time case (see Fig. 7). The overall good agreement in the location of the troughs and ridges between observations and the calculated solution is similar to that found by CE and Held (1984) using similar channel models. Nevertheless, this favorable comparison does not necessarily imply that barotropic models with only topographic forcing are adequate in explaining the 500 mb wave geopotential, nor should it be taken to mean that CE's 6 day damping time scale is appropriate for the atmosphere (see Held, 1984).

With the existence of only one stable equilibrium, the low-frequency variability of the large-scale flow can no longer be explained in terms of transitions from one equilibrium state to another, at least in the present model. In this model, the variability of the stationary wave solution can arise from the variability of the external forcing, namely U^*. (There are other mechanisms for inducing low frequency variability also.) By varying U^*, different equilibrium solutions are calculated. These are plotted in Fig. 8. There is a hint of the existence of "bimodality" in the distribution of the ridges and troughs. The existence of "bimodality" has previously been sought as evidence for the existence of multiple equilibria (see Dole, 1983; Wallace and Blackmon, 1984).

3. Nonlinear bending of resonance curves

The phenomenon of "bent resonance", which arises in some nonlinear models (see Nayfeh and Mook, 1979; Wakata and Uryu, 1984) has sometimes been suggested as an alternative mechanism for multiple equilibria and "bimodality" (e.g., see Speranza, 1985;

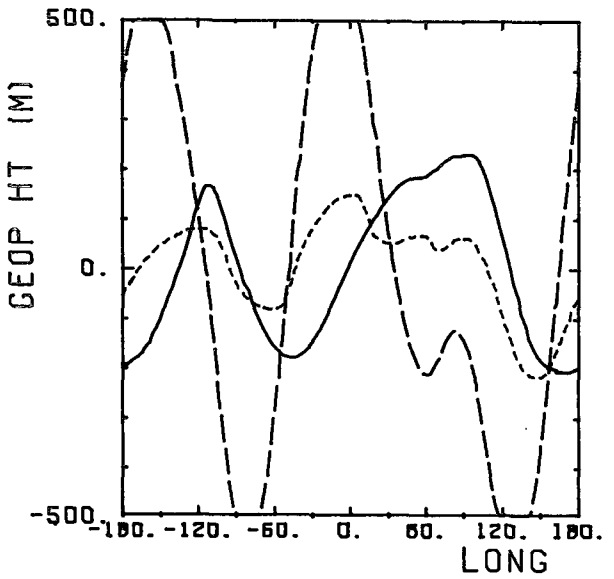

FIG. 7. As in Fig. 6 except for $\tau_E = 14.3$ days.

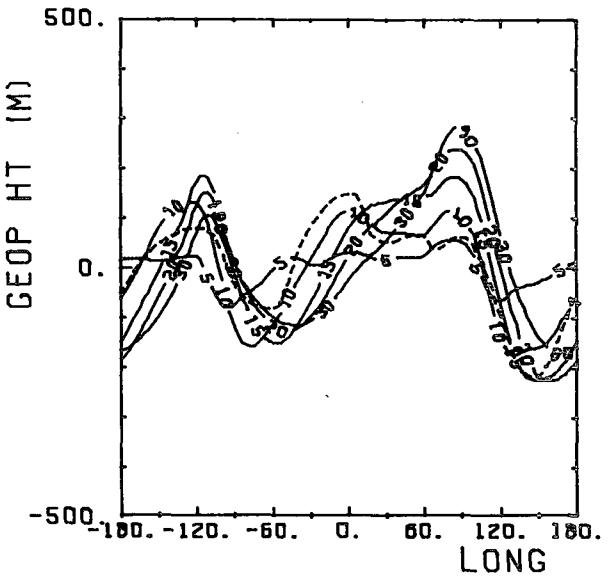

FIG. 8. Wave geopotential height (in meters) at 45°N vs longitude for $\tau_E = 5.7$ days and $U = 5$, 10, 15, 20 and 30 m s^{-1}, as labeled on the curves. The short dashed curve is the observed climatology (Oort, 1983).

Sutera, 1985; Hansen, 1985). In the context of barotropic inviscid models, it suggests that multivalued solutions can exist simultaneously for each zonal index in the region where the resonance curve, such as Fig. 1 or 2, is bent sufficiently by nonlinearity to low values of U as to "tip over". The relevance of such a mechanism to the existence of multiple equilibria is examined here in *dissipative* cases.

There is some indication in the result of Rambaldi and Mo (1984) that bent resonances do occur even in dissipative barotropic models. By comparing our Fig. 2 with Fig. 5, one sees a tendency for the nonlinear mountain torque curve (which, incidentally, also measures the wave amplitude that is out of phase with topography) to be steeper for smaller viscosity on the low-U side of its resonance peak, although it does not yet "tip over" for the two values of damping time used. The question becomes: For damping time scales longer than 14.3 days, can the resonance curve be bent sufficiently that there exist more than one wave solution for each value of U? We will show that the answer is yes (albeit for very weak damping cases), but the additional solutions that result are not *equilibrium solutions* in the presence of damping.

The phenomenon of bent resonance can best be seen when there is only one Fourier mode of topographic forcing. It is also in this context that bent resonances are usually discussed. For this purpose the nonlinear calculation discussed in section 2 is repeated with a topography containing only the dominant mode (m, n) = (2, 1). All h_{mn} are set to zero except h_{21}, which retains its value from the Scripps topography ($\sim$600 m). The nonlinear solution for ϕ_{mn} is again calculated until it converges. The mountain torque now measures the out of phase component of the wave response ϕ_{21}. This is plotted in Fig. 9 for various damping times.

In order to be able to put mountain torque curves calculated with different damping times on the same figure, we have multiplied the ordinate axis by τ_E. Thus the curves are for $-\tau_E \cdot \mathrm{T}$, and the straight line is for $(U^* - U)$. The intersection of the curve with the straight line for each value of τ_E still yields the equilibrium solutions. Keeping this scaling in mind, we see that as τ_E increases the mountain torque first tends to increase in magnitude and then for $\tau_E > 13$ days starts to decrease approximately as $1/\tau_E$. There is no mountain torque in the inviscid limit (i.e., $\tau_E \to \infty$) as the solution of the barotropic equations becomes in phase with the topography.

More importantly, we see in Fig. 9 a clear tendency for the (nonlinear) resonance curve to bend toward low values of U for increasing τ_E. For $\tau_E \gtrsim 15$ days, the phenomenon of nonlinear bending tips the resonance curves over so that 3 values of mountain torque exist on the subresonant side for each value of U. These presumably, are the multiple equilibrium states (also "bimodality", assuming one equilibrium is unstable) referred to by Speranza (1985).

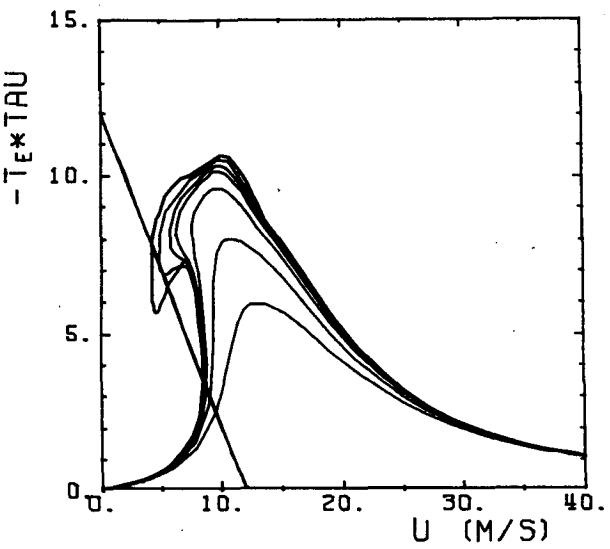

FIG. 9. $-\tau_E \cdot \mathrm{T}$ in m s^{-1}, as a function of U in m s^{-1}. The nonlinear solution is using a one-mode topography: (m, n) = (2, 1), with $|h_{21}| \approx 603$ m. The curves are for, starting from the lowest curve: τ_E = 5, 7, 10, 13, 15, 20 and 30 days. The straight line represents $(U^* - U)$ for $U^* = 12$ m s^{-1}.

However, in the presence of damping, equilibrium solutions only exist at the intersections of the mountain torque curve with the straight line $(U^* - U)$. While it is still possible to have 3 equilibria, these occur for different subresonant values of the zonal index U, and their stability property is such that only one of the equilibria is stable to form-drag instability.

There is a simple way to decide if a particular equilibrium point is stable or not to form-drag instability without having to perform a linear stability (eigenvalue) study as is normally done. It is shown in Tung and Rosenthal (1985) that form-drag instabilities can be decided using the zonal index equation (2.6) alone, which is, in dimensional form

$$\frac{\partial}{\partial t} U = \frac{1}{\tau_E}(U^* - U) + \mathrm{T}(U). \tag{3.1}$$

For westerly U, $\mathrm{T}(U)$ is always negative since mountain torques tend to oppose the zonal flow. Hence $\mathrm{T}(U)$ introduces a deceleration of the zonal index, according to (3.1). This deceleration is balanced by the acceleration introduced by the viscous relaxation term $\tau_E^{-1}(U^* - U)$ for U less than U^*. Away from the equilibrium point, if to its right (i.e. larger values of U) the curve $[-\mathrm{T}(U)]$ has a larger value than the straight line $\tau_E^{-1}(U^* - U)$, the flow decelerates according to (3.1). If in addition, the flow accelerates at the left side of the equilibrium point [i.e., $(-\mathrm{T}(U)$ is lower than $\tau_E^{-1}(U^* - U)$], that particular equilibrium point is stable to form-drag instability. Otherwise the equilibrium is unstable.

As an exercise, let us use CSM's solution displayed as the dashed curve in Fig. 1. For $U^* = 63$ m s^{-1}, the

straight line $\tau_E^{-1}(U^* - U)$ cuts the $[-T(U)]$ curve at 5 different points. Hence there are 5 equilibria. The left-most is a subresonant wavenumber 3 equilibrium. It is stable to form-drag instability because the line $\tau_E^{-1}(U^* - U)$ is higher than the curve $[-T(U)]$ to the left of the equilibrium point and lower to the right. The next intersection is the so-called superresonant wavenumber 3 equilibrium. This is unstable because the line $\tau_E^{-1}(U^* - U)$ is lower than the curve $[-T(U)]$ to the left of the point and higher to the right. The third equilibrium from the left in Fig. 1 is the so-called wavenumber 2 subresonant equilibrium. It is stable by the same arguments as above. The fourth equilibrium from the left is the superresonant wavenumber 2 equilibrium. It is unstable. (Wavenumber 1 resonance is not pronounced, and is hidden on the right shoulder of the wavenumber 2 resonance curve.) The right-most equilibrium is the so-called high zonal-index equilibrium located at $U \approx 63$ m s^{-1}. It is stable because the straight line is higher than the mountain torque curve to the left of the point and lower to the right of the point. These conclusions of stability of equilibria turn out to be the same as those found by CSM (or CD) after lengthy eigenvalue calculations.

Now let us return to Fig. 9. The stability property of the equilibria on the "tipped over" side of the resonance curve turns out to be quite interesting. This can be shown more clearly using a schematic diagram (Fig. 10) which exaggerates the relevant features for the (say, τ_E = 20 day) curve displayed in Fig. 9. For the values of external zonal driving U^* that yield an equilibrium point B below the limit point L, the equilibrium is stable to form-drag instability as indicated by the arrows. The sense of the arrows is deduced from arguments given above. As U^* increases, the equilibrium value of U also increases slowly, until the limit point L is passed. Then for further increases of U^*, U actually *decreases*. What is more interesting however is that the stability of the equilibrium point is also altered when the limit point L is passed. An equilibrium point A above the limit point is unstable to form-drag instability because when perturbed to the small U side, the flow decelerates, and accelerates when perturbed to the larger U side of A. For a fixed value of U^*, a perturbation to the low-U side of A will decelerate the system to the next stable equilibrium point S. No equilibrium points can be found on high-U side of B, so a perturbation to that side can only produce unstable solutions. Thus it is seen that even though it at first appears that for small enough damping the system can possess three equilibria for some values of U^*, it turns out that only one of the equilibria is stable to form-drag instability.

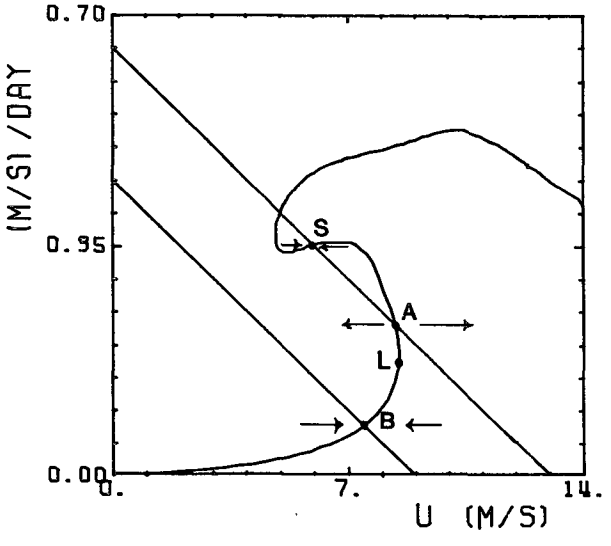

FIG. 10. Mountain torque (−T) in m s^{-1}/day vs U (m s^{-1}) for τ_E = 20 days. L: limit point. B: stable equilibrium below the limit point for U^* = 9 m s^{-1}. A: unstable equilibrium above the limit point for U^* = 13 m s^{-1}. S: stable equilibrium for U^* = 13 m s^{-1}. The arrows indicate the direction of acceleration. Arrows pointing to the right imply acceleration towards larger U, while arrows pointing to the left imply deceleration towards smaller U.

The feature of the mountain-torque curve mentioned above is what make the mechanism of hysteresis possible. Källén (1985) has found from numerical integration of the time-dependent nonlinear barotropic vorticity equation on a sphere that as the external driving U^* is varied the response (e.g., U in our case; the zonal averaged zonal flow at 55°N in his case) does not necessarily follow as it would in the linear case. For the case with a 20-day damping, he finds behavior very similar to what we have just described using Figs. 9 and 10 as far as slow and rapid transitions are concerned. For the low damping case, an increase in external driving U^* first brings on an increase in the response (U corresponding to point B in our Fig. 10). As U^* is increased further the response actually decreases (U passing through the limit point L) first slowly and then more abruptly as the form-drag instability brings on the transition from the unstable equilibrium A to the stable equilibrium S. (In Källén's case, the response in terms of local $\bar{u}$ at 55°N actually *increases* during the last rapid transition mentioned above.)

The wave amplitudes for our case are plotted in Fig. 11. It is seen that as U is first increased from the subresonant side of the resonance curve, the amplitude of the stationary wave solution first increases, as the flow is brought nearer to the resonance peak. The increase in wave amplitude becomes more abrupt as U is brought closer to the limit point L. Then a further increase in driving U^* causes a sudden drop in wave amplitude. It turns out that even though the point S has a larger value of mountain torque than the point B, the point S actually has a wave geopotential height that is only half as large, so that an increase in driving U^* not only causes a reduction in zonal index U, but also a drastic drop in wave amplitude. This is the so-called "jump phenomenon" or "catastrophe" (see Nayfeh and Mook, 1979, p. 168, in association with

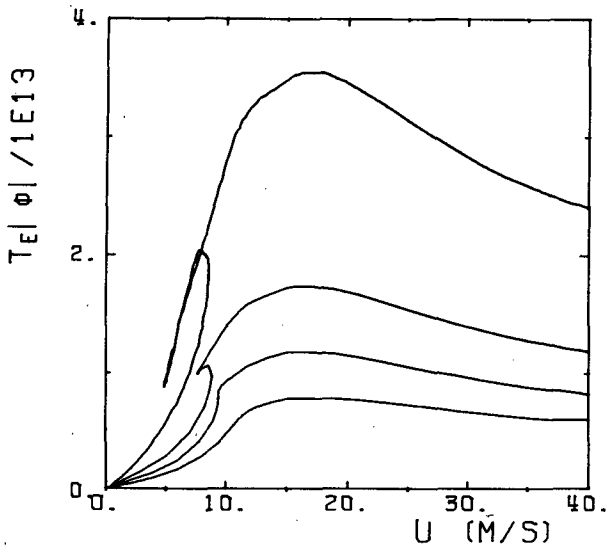

FIG. 11. Amplitude of the nonlinear (2, 1) mode ($|\phi_{21}| \cdot \tau_E/10^{13}$ in m^2) as a function of U in m s^{-1} for τ_E = 5, 7, 10 and 20 days (from bottom to top).

the frequency response of a Duffing oscillator with a "soft" spring).

The case with a larger value of damping behaves as one would expect from linear theory. Both Källén's 5-day damping case and our 5-day damping case show the same unremarkable behavior of the response U following the driving U^*.

In summary, although we find the presence of hysteresis when damping is small enough, only one stable equilibrium is found in our barotropic model. However, the presence of hysteresis can lead to periods of persistence even as external driving is varied, and can also lead to rapid transitions similar to those proposed by CSM from one equilibrium state to another. Källén actually proposes the hysteresis mechanism as a more relevant alternative to theories of multiple equilibria. It should be noted, however, that hysteresis does not become prominent until the damping time is around 20 days or longer. Whether or not the damping timescale for the atmosphere is that long is still a matter of controversy.

Concerning the subject of multiple equilibria, a remark concerning the recent work of Rambaldi and Mo (1984) can be made at this point. They find that for a 15-day Ekman damping time and a one-mode topography there exist in their nonlinear barotropic model 3 equilibria of the same kinds as originally proposed by Charney and DeVore (1979): one low-index subresonant equilibrium, one superresonant unstable equilibrium and one high-index stable equilibrium. No such arrangement of multiple equilibria can be found in our Fig. 9. A major difference between their work and ours is that they implicitly let their zonal index U be damped at a different rate than their stationary waves. Their zonal index is actually damped at $\tau_E/\kappa \approx 36$ days. This in effect makes the straight line $\kappa(U^* - U)/\tau_E$ in Fig. 9 slope at a smaller angle than we have shown in that figure, making it possible to have two additional equilibria on the large-U side of the resonance peak for a U^* between 30 and 40 m s^{-1}. (The value of U^* for multiple equilibria to appear in the model of Rambaldi and Mo is about 10 m s^{-1} smaller than ours. The difference can be attributed to our using 600 m for the topographic mode versus their 400 m.) However, we do not at the present time have an adequate justification for why a different damping time should be applied to the zonal index than to other flow quantities (which include $\bar{u}$). Their selective application of the equivalent barotropic scaling using $\kappa = 0.4$ to the zonal index equation only is seen to be the cause for the existence of multiple equilibria in the model of Rambaldi and Mo.

4. Multiple equilibria in the presence of imposed vorticity source

There is a subtle difference in the way the zonal driving term Ψ^* [appearing in (2.1) and (2.9)] is treated in the present calculation, which is the same as in CSM and Rambaldi and Mo (1984), vis-a-vis the models of CD and Legras and Ghil (1984, 1985). In the former group, Ψ^* is taken as a linear function of y, i.e.

$$\Psi^* = -U^* y, \tag{4.1}$$

so that the driving term shows up only in the zonal index equation (2.6), and not as a vorticity source in the barotropic vorticity equation (2.1). In the latter group, Ψ^* is taken to be a basis eigenfunction of the Laplace equation. In CD for example, Ψ^* is written as

$$\Psi^* = \Psi_A^* \sqrt{2} \cos y. \tag{4.2}$$

Consequently, the driving term not only shows up as a zonal momentum driving in the zonal index equation, since from (2.9)

$$U^* \equiv \frac{1}{y_2 - y_1} [\Psi^*|_{y_1} - \Psi^*|_{y_2}]$$

$$= \frac{2\sqrt{2}}{(y_2 - y_1)} \Psi_A^*,$$

but it also appears as a vorticity source in the barotropic vorticity equation, since

$$\nabla^2 \Psi^* = \frac{-1}{L^2} \Psi_A^* \sqrt{2} \cos y$$

is not zero for (4.2) but vanishes for (4.1). For a Ψ^* that is independent of x, the difference between the two types of treatment is inconsequential in truncated (quasi-linear) models, but can become significant in nonlinear models. This difference is, in our opinion, why Legras and Ghil (1984, 1985) found multiple equilibria in their nonlinear model for some values of zonal driving, while we find only a single equilibrium for all values of U^* under otherwise similar conditions.

In this section, we will first demonstrate using our channel model that a strong enough vorticity source can cause the state of multiple equilibria to occur and we will discuss the mechanism through which the vorticity source acts to produce the multiple equilibria found. It then naturally leads to the questions: "What is the physical basis for the zonal driving term and the vorticity source?" "What is the realistic range of values for these quantities for the atmosphere?" These issues will be addressed in section 5.

We will adopt here a zonal driving profile of the form

$$\Psi^* = -U^* y + \frac{\omega^*}{\pi}(y_2 - y_1)\sin 2\pi[y/(y_2 - y_1)] \quad (4.3)$$

so that when $2\omega^* = U^*$, the zonal flow associated with (4.3)

$$u^* \equiv -\frac{\partial}{\partial y}\Psi^* = U^* - 2\omega^* \cos 2\pi[y/(y_2 - y_1)]$$

resembles an internal jet of the form

$$u^* = U^*\left[1 - \cos 2\pi\left(\frac{y}{y_2 - y_1}\right)\right], \quad (4.4)$$

very similar to that given by (4.2). There are two advantages in using (4.3) instead of (4.2). First, as we will show in section 5, the zonal driving term U^* in the zonal index equation and the vorticity source $\nabla^2\Psi^*$ in the barotropic vorticity equation have different physical origins, and it is not appropriate to have them related by a single parameter Ψ_A^*. The two parameters U^* and ω^* can be separately varied in (4.3). Second, the form (4.3) is of the form given by (2.15a) that we use to expand our solutions in and so technically it is more advantageous to use (4.3) instead of (4.2) in our present formulation. In any case, the results using (4.2) can be reproduced approximately if we specialize to the case of

$$U^* = 2\omega^*. \quad (4.5)$$

The internal jet represented by (4.4) has a jet maximum given by

$$u^*_{\max} = 2U^* = 4\omega^*.$$

In Figs. 12 to 15, we present results calculated using the same one-mode topography as used in section 3, for various values of vorticity source ω^*, and for damping times ranging from $\tau_E = 5$ to 15 days. In general, the mountain torque curves shown increase in amplitude as ω^* is increased, and the phenomenon of resonance bending also becomes more pronounced for larger values of ω^*. For $\tau_E = 5$ days, we find only one equilibrium in Fig. 12 even for an internal jet with $u^*_{\max}$ as large as 80 m s^{-1}. The same situation holds for $\tau_E = 7$ and 10 days as shown in Figs. 13 and 14, respectively. For $\tau_E = 15$ days, small protrusions from the mountain torque curve become more evident for

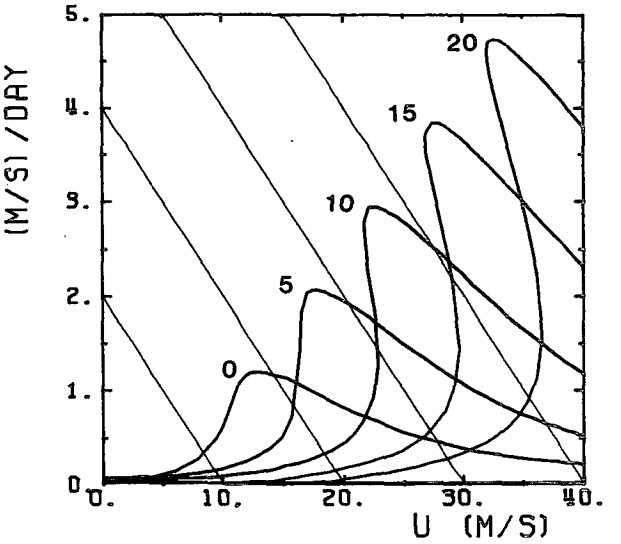

FIG. 12. Mountain torque (−T) in m s^{-1}/day vs U (m s^{-1}) for $\omega^* = 0$, 5, 10, 15 and 20 m s^{-1} for $\tau_E = 5$ days and $|h_{21}| = 603$ m. The straight lines are $\tau_E^{-1}(U^* - U)$ with $U^* = 2\omega^*$.

large values of $u^*_{\max}$, as shown in Fig. 15. [These features will be explained in a moment.] There is however still no multiple equilibria for $u^*_{\max}$ as large as 80 m s^{-1} if the relationship (4.5) is required to hold. If U^* and ω^* are treated as independent parameters, then it is possible to find multiple equilibria in Fig. 15 for $4\omega^* = 80$ m s^{-1} and U^* tuned to be between 40 and 50 m s^{-1}.

For even larger values of $u^*_{\max}$, it becomes possible to have multiple equilibria even if relationship (4.5) is required to hold. In Fig. 16 we show that for $\tau_E = 10$ days and $U^* = 2\omega^* = 80$ m s^{-1}, three equilibria are found. In Fig. 17, we find 5 equilibria for $U^* = 2\omega^* = 80$ m s^{-1} in the presence of a 15 day damping. It should be pointed out that these values of external driving correspond to an internal jet with a 160 m s^{-1} wind speed. We will show in section 5 that such large values of vorticity source and zonal driving cannot be justified for our atmosphere.

Comparing results in section 4 with those in section 3, we see that the additional equilibria are due to the presence of vorticity source in the interior of the channel adopted in the present section. With the vorticity source taken to be in the form of a meridional jet, a mean *shear* is induced even in the absence of topographic waves. In the presence of a mean shear in the basic state, even the linear solution cannot be written in terms of a simple sinusoidal mode. The mountain torque, obtained as the projection of the forced solution onto the sinusoidal mode of the topography, will include contributions from higher harmonics. These projections from higher (nonsinusoidal) modes onto the sinusoidal mode of the topography are responsible for the appearance of the small protrusions on the mountain torque curve.

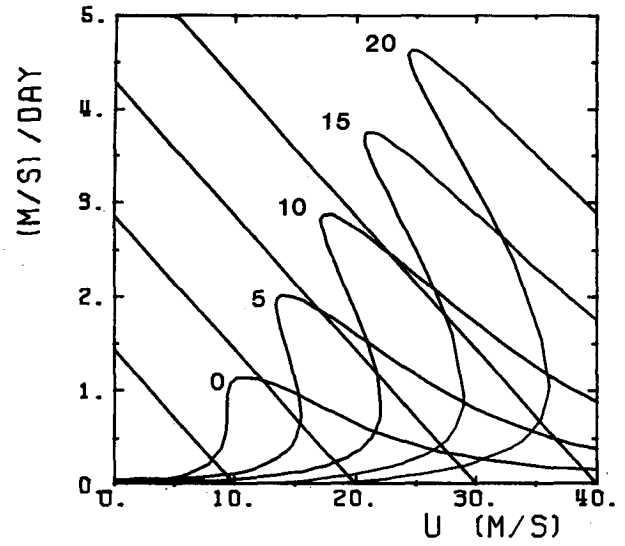

FIG. 13. As in Fig. 12 except for τ_E = 7 days.

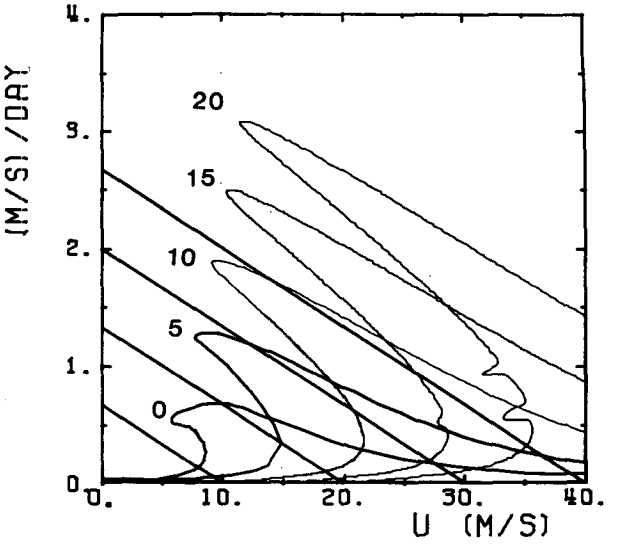

FIG. 15. As in Fig. 12 except for τ_E = 15 days.

5. Physical basis for U^* and $\nabla^2\Psi^*$

It is generally accepted that in the presence of damping, a vorticity source is needed in the barotropic vorticity equation (2.1) in order to maintain a nontrivial steady state flow in a channel with rigid walls. Similarly an external zonal driving term U^* is needed in the zonal index equation (2.6). (Otherwise $U = 0$ will be the only steady state solution to that equation.) It is often suggested that these "external" forcing terms are thermal in origin and so cannot be determined within barotropic models. It is further assumed by some authors that these terms are arbitrary as far as barotropic models are concerned, with the consequence that values for U^* greater than 60 m s^{-1} and internal jets with winds exceeding 150 m s^{-1} have been used with no physical justification given.

We have seen from the preceding sections that the existence of multiple equilibria in some barotropic models depends on these external forcing parameters taking on some rather large values, which we will show to be unrealistic.

a. *The physical interpretation for U^**

Rambaldi (1982) and Källén (1983) suggested that the parameter U^* appearing in barotropic models can probably be interpreted as arising from the flux of momentum from the tropics. A systematic derivation of

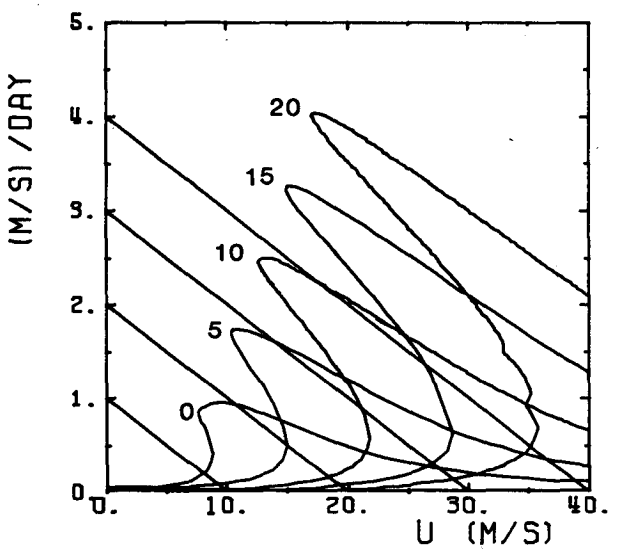

FIG. 14. As in Fig. 12 except for τ_E = 10 days.

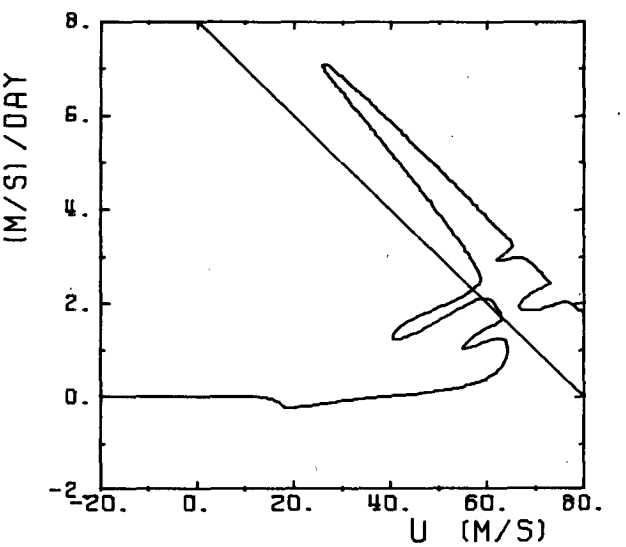

FIG. 16. As in Fig. 12 except for τ_E = 10 days and ω^* = 40 m s^{-1}.

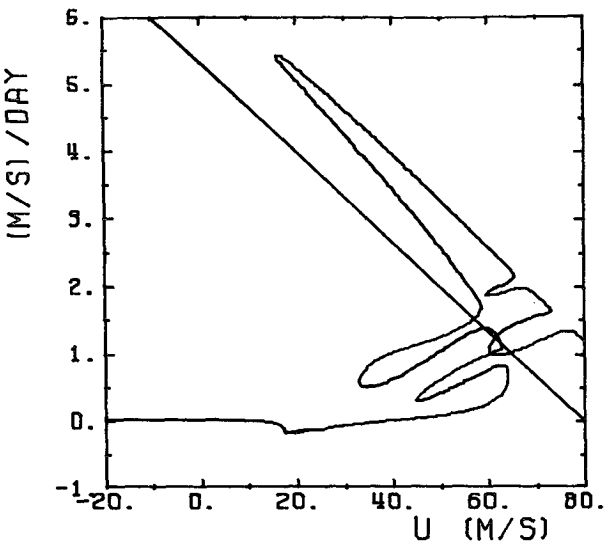

FIG. 17. As in Fig. 12 except for τ_E = 15 days and ω^* = 40 m s^{-1}.

U^* starting with a three-dimensional model was given by Tung and Rosenthal (1985). An explicit expression for U^* was found in terms of the density-weighted vertical integral of the zonal mean lateral flux of angular momentum into the channel. This physical interpretation allows us to infer a value of the order of U^* $\sim$ 2 to 4 m s^{-1}, using the observed climatology for transient eddy momentum fluxes from Lau (1979).

We will give below an alternate derivation which turns out to be simpler and more general. (The quasi-geostrophic approximation used in Tung and Rosenthal (1985) is not needed for the present derivation.) Our purpose in giving this derivation here is to more clearly show that the physical origin of U^* is not "thermal", as we will not have to use the energy equation in our derivation.

It turns out that an equation for the zonal index can be derived for a three-dimensional atmosphere using only the zonal momentum equation, and that the resulting equation is almost identical to Eq. (2.6) derived earlier for a barotropic atmosphere.

Let M be the absolute angular momentum in the east–west direction, i.e.

$$M = (\Omega a \cos\theta + u)a \cos\theta,$$

where a is the radius of the earth, Ω the angular speed of the earth's rotation, θ the latitude and u the relative velocity of the atmosphere in the east–west direction. The statement of angular momentum balance can be expressed in pressure coordinates, as

$$\frac{d}{dt}M = -g\frac{\partial}{\partial\lambda}z + a\cos\theta F_\lambda \qquad (5.1)$$

[see Lorenz (1967) for a derivation of (5.1) in height coordinates; the conversion to pressure coordinates is straightforward]. In (5.1) λ is the longitude, z the geopotential height at constant pressure and F_λ is the frictional force in the east–west direction. When integrated in an atmospheric volume defined by $0 \leqslant \lambda \leqslant 2\pi$, $\theta_1 \leqslant \theta \leqslant \theta_2$ and $0 < p \leqslant p_s$, (5.1) becomes

$$\frac{\partial}{\partial t}\iiint_V M dV + \iint_S M\mathbf{v}\cdot\mathbf{n}dS = -g\iiint_V \frac{\partial}{\partial\lambda}z dV + \iiint_V a\cos\theta F_\lambda dV, \qquad (5.2)$$

where S is the boundary surface of V and $\mathbf{n}$ is the outward unit normal of S. The first term in (5.2) can be written as

$$\frac{\partial}{\partial t}\iiint_V M dV = \frac{\partial}{\partial t}\int_{\theta_1}^{\theta_2} d\theta \int_0^{2\pi} d\lambda \int_0^{p_s} dpua^2\cos\theta \approx \frac{\partial}{\partial t}\int_{\theta_1}^{\theta_2} d\theta \int_0^{1000\text{ mb}} dp 2\pi a^2 \bar{u}\cos\theta. \qquad (5.3)$$

In obtaining (5.3), we have assumed that the total mass in V does not change appreciably, so that the rate of change of the absolute angular momentum is due essentially to the change in relative angular momentum. We have also approximated the surface pressure p_s by p_{00} = 1000 mb in taking the zonal average of the angular momentum ($\bar{u} \equiv (2\pi)^{-1}\int_0^{2\pi} u d\lambda$). Since there is no normal velocity through the top and bottom of V, the momentum flux [the second term in (5.2)] is due mainly to the meridional flux of zonal momentum across the vertical "walls", θ_1 and θ_2. i.e.

$$\iint_S M\mathbf{v}\cdot\mathbf{n}dS = \int_0^{2\pi}\int_0^{p_s} Mv|_{\theta_1}^{\theta_2} dp \approx 2\pi a\int_0^{1000\text{ mb}} \overline{uv}\cos\theta|_{\theta_1}^{\theta_2} dp. \qquad (5.4)$$

(We have again assumed the net shift in mass across a latitude belt is small).

The third term in (5.2) is the so-called mountain torque term. It would have been zero had it not been for the fact that the lower surface, $z = h(\lambda, \theta)$, is not a constant pressure surface and that in general there may be net pressure differences between the east and west sides of mountain ranges. Since (see Wahr and Oort, 1984):

$$\int_0^{p_s}\left(\frac{\partial z}{\partial\lambda}\right)dp = \frac{\partial}{\partial\lambda}\left(\int_0^{p_s} z dp\right) - h\frac{\partial p_s}{\partial\lambda},$$

the mountain torque term can be reexpressed as

$$-g\iiint_V \frac{\partial}{\partial\lambda}z dV = -g\int_0^{2\pi} d\lambda\int_{\theta_1}^{\theta_2} d\theta a^2 \times\cos\theta\int_0^{p_s}\frac{\partial z}{\partial\lambda}dp = 2\pi a^2 g\int_{\theta_1}^{\theta_2}\overline{h\frac{\partial p_s}{\partial\lambda}}d\theta. \qquad (5.5)$$

The last term in (5.2) is the so-called frictional torque term. Since F_λ is a surface force, it can be expressed in the form of a divergence of a stress τ_λ. Converting the volume integral into a surface integral and neglecting the surface stress term except at the lower surface, where the normal component of τ_λ is $\tau_\lambda{}^0$ we find

$$\iiint_V a\cos\theta F_\lambda dV = \int_{\theta_1}^{\theta_2} d\theta \bar{\tau}_\lambda{}^0 \cdot 2\pi a^3 \cos^2\theta. \quad (5.6)$$

Substituting (5.3)–(5.6) into (5.2), we now have upon division by $2\pi a^2$,

$$\frac{\partial}{\partial t}\int_0^{1000\text{ mb}} dp \int_{\theta_1}^{\theta_2} \bar{u}\cos\theta d\theta = \int_0^{1000\text{ mb}} dp \frac{1}{a}\overline{uv} \times \cos\theta|_{\theta_2}^{\theta_1} + \int_{\theta_1}^{\theta_2} d\theta\left[a\bar{\tau}_\lambda{}^0\cos^2\theta + g\frac{\overline{h\partial p_s}}{\partial\lambda}\right]. \quad (5.7)$$

Equation (5.7) states that the rate of change of the zonal mean angular momentum inside the "channel", $\theta_1 \leqslant \theta \leqslant \theta_2$ is given by the meridional eddy flux of zonal momentum into the region from south of θ_1 and north of θ_2, plus the total torque exerted on the atmosphere by the underlying surface of the earth. The surface torque consists of friction torque and mountain torque, given by the first and second term in the brackets, respectively. Now if we restrict our attention to a mid-latitude β-plane channel and replace the trigonometric function $\cos\theta$ by $\cos\theta_0$, then (5.7) becomes, upon division by $\cos\theta_0 \cdot (\theta_2 - \theta_1)p_{00}$:

$$\frac{\partial}{\partial t}\int_0^{p_{00}} U dp/p_{00} = \left\{\frac{1}{\tau_E}(U^* - U) + \mathrm{T}(U)\right\}\Big|_{z_1}, \quad (5.8)$$

where

$$U \equiv \frac{1}{\theta_2 - \theta_1}\int_{\theta_1}^{\theta_2} \bar{u} d\theta$$

$$\frac{1}{\tau_E}U^* \equiv \int_0^{p_{00}} \frac{dp}{p_{00}} \frac{1}{a(\theta_2 - \theta_1)} \overline{uv}|_{\theta_2}^{\theta_1} \quad (5.9)$$

$$T(U) \equiv \frac{g}{p_{00}(\theta_2 - \theta_1)}\int_{\theta_1}^{\theta_2} d\theta \frac{\overline{h\partial p_s}}{\partial\lambda} = \frac{f_0}{H_0(\theta_2 - \theta_1)}\int_{\theta_1}^{\theta_2} \overline{hv_0} d\theta. \quad (5.10)$$

To obtain (5.8), we have used the Ekman boundary layer solution to obtain a relation between the surface frictional stress $\bar{\tau}_\lambda{}^0$ and the geostrophic component of the zonal wind at the top of the Ekman boundary layer (see Charney and Eliassen, 1949). The Ekman damping time τ_E is defined by (2.4). In the definition for the mountain torque, v_0 is used to denote the geostrophic component of the meridional velocity, defined through

$$f_0 v_0 = \frac{1}{\rho_0 a\cos\theta_0}\frac{\partial}{\partial\lambda}p_s.$$

The right-hand side of Eq. (5.8) is to be evaluated at the top of the Ekman layer, z_1.

Equation (5.8) implies that at an equilibrium the zonal momentum driving $\tau_E{}^{-1}U^*$ should balance the friction torque $\tau_E{}^{-1}U$ and the mountain torque T(U). i.e.

$$\frac{1}{\tau_E}U^* = \frac{1}{\tau_E}U - \mathrm{T}(U). \quad (5.11)$$

The solution to (5.11) then yields the equilibrium mean flow U at $z = z_1$. Eq. (5.11) is of the same form as the mean flow in some barotropic models [see especially CSM's Eq. (3) and our Eq. (2.14)]. It is clear from our derivation that Eq. (5.11) is of more general applicability and not limited to barotropic models.

Of particular interest for our present purpose is the physical definition of U^* given by (5.9). Using the observed zonal momentum flux at $\theta_1 = 30°$N (The momentum flux at $\theta_2 = 63°$N is negligible) from Lau (1979), we find

$$\int_0^{p_{00}} \overline{uv\cos\theta}|_{\theta_1}^{\theta_2}\frac{dp}{p_{00}} \approx 16\text{ m}^2\text{ s}^{-2},$$

yielding a zonal momentum driving of

$$\frac{1}{\tau_E}U^* \approx 4\times 10^{-6}\text{ m s}^{-2}. \quad (5.12)$$

If a typical Ekman damping time scale of 6 days is used for τ_E (see Charney and Eliassen, 1949), the zonal driving velocity is found to be

$$U^* \approx 2\text{ m s}^{-1},$$

which should be compared to $U^* \approx 63$ m s^{-1} used by CSM. (It should be pointed out however that in the barotropic model formulation used by CSM, their U^* should be interpreted as the zonal driving for the mean wind at some "equivalent barotropic" level, not necessarily near the surface. Therefore, one can conceivably add about 20 m s^{-1} to our estimate for U^* to account for the difference between the surface flow and the flow at the "equivalent barotropic" level.)

An alternative estimate of U^* can also be obtained using the estimate by Wahr and Oort (1984) of the total torque [the last integral in Eq. (5.7)]. They find that for $\theta_1 = 30°$N and $\theta_2 = 63°$N the total torque is roughly 4×10^{-6} to 5×10^{-6} m s^{-2} for climatological winters. This is very close to (5.12) based on the observed zonal momentum flux at 30°N (Lau, 1979).

Given the observational evidence from Wahr and Oort (1984) and Newton (1971) that the friction torque is about 4 times larger than the mountain torque in these latitudes, it appears that at equilibrium the dominant balance is between friction torque and zonal driving. Such a balance is not likely to yield more than one solution in equilibrium U. Furthermore, the approximate solution inferred from such a balance, i.e.

$$\frac{1}{\tau_E}U \sim \frac{1}{\tau_E}U^*$$

yields

$$U \sim 2 \text{ m s}^{-1},$$

which is close to the observed climatological net zonal wind at the top of the Ekman layer between latitudes 30 and 63°N.

b. A physical basis for the vorticity source used in barotropic models

Because barotropic models cannot be derived rigorously from governing physical equations, which are baroclinic, the derivation of the vorticity source used in barotropic models is necessarily less systematic. We will adopt in the following the approach first used by Charney and Eliassen (1949) in their derivation of the "equivalent barotropic model" starting from the three-dimensional quasi-geostrophic potential vorticity equation:

$$\rho_0 \frac{D}{Dt}[\nabla^2\Psi + \beta y] = f_0 \frac{\partial}{\partial z}(\rho_0 w), \qquad (5.13)$$

where

$$\frac{D}{Dt} \equiv \frac{\partial}{\partial t} + J[\Psi, \,].$$

Equation (5.13) is then vertically integrated from the top of the Ekman layer z_1 to ∞, to yield

$$\frac{1}{H_0\rho_0(z_1)} \int_{z_1}^{\infty} dz \rho_0 \frac{D}{Dt}[\nabla^2\Psi + \beta y]$$

$$= \frac{-f_0}{H_0} J[\Psi, h] - \frac{1}{\tau_E}\nabla^2\Psi. \qquad (5.14)$$

The right-hand side of (5.14) is to be evaluated at z_1.

The "equivalent barotropic" assumption put forth first by Charney and Eliassen (1949) is to assume the existence of a level (~500 mb) where the left-hand side of (5.14) becomes

$$\frac{D}{Dt}[\nabla^2\Psi + \beta y]$$

when evaluated at this "equivalent barotropic level". Thus the equivalent barotropic equation is

$$\frac{D}{Dt}[\nabla^2\Psi + \beta y] = -\frac{f_0}{H_0} J[\Psi, h] - \frac{1}{\tau_E}\nabla^2\Psi. \qquad (5.15)$$

Strictly speaking, the two-sides of this equation are each evaluated at a different level: the left-hand side at the equivalent barotropic level and the right-hand side at the top of the Ekman layer. Such a difference is sometimes ignored to arrive at the barotropic vorticity equation similar to the one we are considering [cf. Eq. (2.1)]. Alternatively, a scaling factor $\kappa \approx 0.4$ is sometimes introduced in the right-hand side to account for the difference in the flow speeds at the two-levels, resulting in an "equivalent barotropic" model. In either case, however, it is seen that a vorticity source $\nabla^2\Psi^*$ is absent from Eq. (5.15).

It appears then that there is no obvious origin for the vorticity source often introduced into the barotropic vorticity equation. The notion that the vorticity source used in barotropic models is to be attributed to baroclinic (or thermal) origin is probably without firm physical basis.

The need to introduce such a source in barotropic models with damping is also not clearly demonstrated. While it is true that without a source term, flow inside a channel will spin down under the action of (Ekman) damping and so no (nontrivial) steady state can be maintained, it should be pointed out (see also Tung and Rosenthal, 1985) that this is only a result of the artificial rigid channel boundary condition adopted by most authors. We see from section 5a that the angular momentum budget for the real atmosphere is such that there is a net lateral zonal momentum flux into a mid-latitude channel from the tropics. It has been shown in Tung and Rosenthal that such a flux (U^*) is capable of maintaining the kind of westerly flow that is observed north of 30°N. Therefore it appears that in order to mimic the angular momentum budget of the real atmosphere in a model one should modify the lateral channel boundary condition to allow the flux of transient eddy momentum to pass through. This will lead to the zonal driving term U^* in the zonal index equation (2.6). This term alone will be sufficient to maintain the momentum budget of the midlatitude channel without an ad hoc vorticity source term in the barotropic vorticity equation (2.1).

Perhaps if Eq. (5.15) is further averaged with respect to time a vorticity source due to the transient eddy flux of vorticity can arise in the interior of the channel as a forcing term for the time-averaged flow. However, it is inconceivable that such an eddy forcing in the lower atmosphere can achieve a jet speed of the magnitude needed for multiple equilibria to exist.

6. Conclusion

The concept of wavy equilibrium first put forth by Charney and DeVore (1979) is an interesting one. It suggests that certain arrangements of the large-scale wave-mean flow system can result in a state that has some persistence in the absence of changes in external forcing. This mechanism can perhaps explain some features of the blocking phenomenon in the atmosphere, as suggested by Charney and DeVore (1979), Charney *et al.* (1981) and many others.

Based on results from highly-truncated models, Charney and DeVore further suggested that more than one such equilibrium for a given forcing can exist, and that the transitions between one or the other equilibrium should probably correspond to certain blocked and unblocked situations in the atmosphere. We wish to remark here that firstly, as far as accounting for the

variability of the large-scale flow pattern is concerned, there is no need to invoke the mechanism of multiple equilibria. Since the so-called external forcing parameters are variable, their variability can induce variability in the wavy "equilibrium" even if there is only one such "equilibrium". Second, by relaxing the severe truncations used in early models, we have found that the state of multiple equilibria of large-scale flow disappears in our nonlinear model.

We have by no means ruled out the possibility of multiple equilibria and indeed we can show that they exist in some parameter regime. We have attempted in the present article to show that the parameter regime where multiple equilibria have been found in barotropic models is probably far from realistic. Nevertheless, physical ambiguities inherent in barotropic models, which cannot be rigorously derived from first principles, probably can allow some versions of the models to produce multiple equilibria. For example, we have shown that if one makes some ad hoc modification to the barotropic vorticity equation using the scaling factor κ selectively applied to some terms and not others, multiple equilibria appear even in nonlinear models without severe truncation (cf. Rambaldi and Mo, 1984). Since this κ factor specifically concerns the effect of vertical shear of the flow in the atmosphere, we feel that this issue should not be addressed using a barotropic model. A more consistent resolution should be obtained with an appropriate baroclinic model. Our results to be presented in Part II dealing with baroclinic models suggest that it is also unlikely for multiple equilibria to exist.

Acknowledgments. The authors would like to thank Dr. Werner C. Rheinboldt and Mr. John V. Burkardt for kindly making available to them their PITCON subroutine used in the numerical location of the nonlinear equilibrium solutions (for a description of PITCON, see Rheinboldt and Burkardt, 1983a,b).

Present research is sponsored by the National Science Foundation GARP, under grant ATM8217616. A portion of the computation was performed on the CRAY computer at the National Center for Atmospheric Research, also sponsored by NSF.

REFERENCES

Charney, J. G., and A. Eliassen, 1949: A numerical method for predicting the perturbations of the middle latitude westerlies. *Tellus*, **1**, 38–54.

——, and J. G. DeVore, 1979: Multiple flow equilibria in the atmosphere and blocking. *J. Atmos. Sci.*, **36**, 1205–1216.

——, and D. M. Straus, 1980: Form-drag instability, multiple equilibria and propagating planetary waves in baroclinic, orographically forced, planetary wave systems. *J. Atmos. Sci.*, **37**, 1157–1176.

——, J. Shukla and K. C. Mo, 1981: Comparison of a barotropic blocking theory with observation. *J. Atmos. Sci.*, **38**, 762–779.

Davey, M. K., 1980: A quasi-linear theory for rotating flow over topography. Part 1. Steady β-plane channel. *J. Fluid Mech.*, **99**, 267–292.

——, 1981: A quasi-linear theory for rotating flow over topography. Part 2. Beta-plane annulus. *J. Fluid Mech.*, **103**, 297–320.

Dole, R. M., 1983: Persistent anomalies of the extratropical Northern Hemisphere wintertime circulation. *Large-Scale Dynamical Processes in the Atmosphere*, B. J. Hoskins and R. P. Pearce, Eds. Academic Press, 397 pp.

Gates, W. L., and A. B. Nelson, 1975: A new (revised) tabulation of Scripps topography on a 1° global grid. Part I: Terrain heights. The Rand Corp., R-1276-1-ARPA, 140 pp.

Hansen, A. R., 1985: Observational characteristics of atmospheric planetary waves with bimodal amplitude distribution. Workshop in Large-Scale Anomalies and Blocking, *Advances in Geophysics*, to appear.

Hart, J. E., 1979: Barotropic quasi-geostrophic flow over anisotropic mountains. *J. Atmos. Sci.*, **36**, 1736–1746.

Held, I. M., 1984: Stationary and quasi-stationary eddies in the extratropical troposphere: Theory. *Large-Scale Dynamical Processes in the Atmosphere*, B. J. Hoskins and R. P. Pearce, Eds., Academic Press.

Källén, E., 1981: The nonlinear effects of orographic and momentum forcing in a low-order barotropic model. *J. Atmos. Sci.*, **38**, 2150–2163.

——, 1982: Bifurcation properties of quasi-geostrophic, barotropic models and their relation to atmospheric blocking. *Tellus*, **34**, 255–265.

——, 1983: A note on orographically induced instabilities in two-layer models. *J. Atmos. Sci.*, **40**, 500–505.

——, 1985: On hysteresis-like effects in orographically forced models. *Tellus*, May issue.

Kanamitsu, M., 1981: Some climatological and energy budget calculations using the FGGE III-b analyses during January 1979. *Dynamic Meteorology: Data Assimilation Methods*, L. Bengtsson, M. Ghil, E. Källén, Eds., Springer Verlag, 263–318.

Keller, H. B., 1977: Numerical solution of bifurcation and nonlinear eigenvalue proglems. *Applications of Bifurcation Theory*, P. Rabinowitz, Ed., Academic Press, 359–384.

Lau, N. C., 1979: The observed structure of tropospheric stationary waves and the local balances of vorticity and heat. *J. Atmos. Sci.*, **36**, 996–1016.

Legras, B., and M. Ghil, 1984: Blocking and variations in atmospheric predictability. *Predictability of Fluid Motions*, G. Holloway and B. J. West, Eds., Amer. Inst. Phys., 612 pp.

——, and ——, 1985: Persistent anomalies, blocking and variations in atmospheric predictability. *J. Atmos. Sci.*, **42**, 433–471.

Lorenz, E. N., 1967: *The Nature and Theory of the General Circulation of the Atmosphere.* World Meteorological Organization, 161 pp.

Nayfeh, A. H., and D. T. Mook, 1979: *Nonlinear Oscillations.* Wiley, 704 pp.

Newton, C. W., 1971: Mountain torques in the global angular momentum balance. *J. Atmos. Sci.*, **28**, 623–628.

Oort, A. H., 1983: Global Atmospheric Circulation Statistics, 1958–1973, NOAA Prof. Paper No. 14, U.S. Govt. Printing Office, Washington, DC, 180 pp.

Pedlosky, J., 1981a: Resonant topographic waves in barotropic and baroclinic flows. *J. Atmos. Sci.*, **38**, 2626–2641.

——, 1981b: The nonlinear dynamics of baroclinic wave ensembles. *J. Fluid Mech.*, **102**, 169–209.

Pierrehumbert, R. T., and P. Malguzzi, 1984: Forced coherent structures and local multiple equilibria in a barotropic atmosphere. *J. Atmos. Sci.*, **41**, 246–257.

Rambaldi, S., 1982: Multiple equilibria and their stability in a barotropic and baroclinic atmosphere. Ph.D. thesis, M.I.T., Cambridge, MA 02139.

——, and K. C. Mo, 1984: Forced stationary solutions in a barotropic channel: Multiple equilibria and theory of nonlinear resonance. *J. Atmos. Sci.*, **41**, 3135–3146.

Reinhold, B. B., and R. T. Pierrehumbert, 1982: Dynamics of weather regimes: Quasi-stationary waves and blocking. *Mon. Wea. Rev.*, **110**, 1105–1145.

Rheinboldt, W. C., and J. V. Burkardt, 1983a: A locally parameterized continuation process. *A.C.M. Transactions on Mathematical Software,* **9,** 215–235.

——, and ——, 1983b: Algorithm 596: A program for a locally parameterized continuation process. *A.C.M. Transactions on Mathematical Software,* **9,** 236–241.

Roads, J. O., 1980a: Stable near-resonant states forced by perturbation heating in a simple baroclinic model. *J. Atmos. Sci.,* **37,** 1958–1967.

——, 1980b: Stable near-resonant states forced by orography in a simple baroclinic model. *J. Atmos. Sci.,* **37,** 2381–2395.

——, 1982: Stable and unstable near-resonant states in multi-level severely truncated, quasi-geostrophic models. *J. Atmos. Sci.,* **39,** 203–224.

Speranza, A., 1985: Deterministic and statistical properties on Northern Hemisphere, middle-latitude circulation: Minimal theoretical models. Workshop in Large-Scale Anomalies and Blocking, *Advances in Geophysics,* to appear.

Sutera, A., 1985: Probability density distribution of large-scale atmospheric flow. Workshop in Large-Scale Anomalies and Blocking, *Advances in Geophysics,* to appear.

Trevisan, A., and A. Buzzi, 1980: Stationary response of barotropic weakly nonlinear Rossby waves to quasi-resonant orographic forcing. *J. Atmos. Sci.,* **37,** 947–957.

Tung, K. K., and A. J. Rosenthal, 1985: On the extended-range predictability of large-scale quasi-stationary patterns in the atmosphere. *Tellus,* to appear.

Wahr, J. M., and A. H. Oort, 1984: Friction and mountain-torque estimates from global atmospheric data. *J. Atmos. Sci.,* **41,** 190–204.

Wakata, Y., and M. Uryu, 1984: Quasi-resonant Rossby wave. Part I: External Wave. *J. Meteor. Soc. Japan,* **62,** 388–412.

Wallace, J. M., and M. L. Blackmon, 1984: Observations of low-frequency atmospheric variability, in *Large-Scale Dynamical Processes in the Atmosphere,* B. J. Hoskins and R. P. Pearce, Eds., Academic Press, 397 pp.

Wiin-Nielson, A., 1979: Steady states and stability properties of a low order barotropic system with forcing and dissipation. *Tellus,* **31,** 375–386.

Yoden, S., 1983a: Nonlinear interactions in a two-layer, quasi-geostrophic, low-order model with topography. Part I: Zonal flow-forced wave interactions. *J. Meteor. Soc. Japan,* **61,** 1–18.

——, 1983b: Nonlinear interactions in a two-layer, quasi-geostrophic, low-order model with topography. Part II: Interactions between zonal flow, forced waves and free waves. *J. Meteor. Soc. Japan,* **61,** 19–35.

——, 1985: Bifurcation properties of a quasi-geostrophic, barotropic, low-order model with topography. *J. Meteor. Soc. Japan,* to appear.